# Brownian Dynamics Simulations of Interactions between Aldolase and G- or F-Actin

Igor V. Ouporov,* Harvey R. Knull,# and Kathryn A. Thomasson*
Departments of *Chemistry and #Biochemistry and Molecular Biology, University of North Dakota, Grand Forks, North Dakota 58202 USA

ABSTRACT Compartmentation of proteins in cells is important to proper cell function. Interactions of F-actin and glycolytic enzymes is one mechanism by which glycolytic enzymes can compartment. Brownian dynamics (BD) simulations of the binding of the muscle form of the glycolytic enzyme fructose-1,6-bisphosphate aldolase (aldolase) to F- or G-actin provide first-encounter snapshots of these interactions. Using x-ray structures of aldolase, G-actin, and three-dimensional models of F-actin, the electrostatic potential about each protein was predicted by solving the linearized Poisson-Boltzmann equation for use in BD simulations. The BD simulations provided solution complexes of aldolase with F- or G-actin. All complexes demonstrate the close contacts between oppositely charged regions of the protein surfaces. Positively charged surface regions of aldolase (residues Lys 13, 27, 288, 293, and 341 and Arg 257) are attracted to the negatively charged amino terminus (Asp 1 and Glu 2 and 4) and other patches (Asp 24, 25, and 363 and Glu 361, 364, 99, and 100) of actin subunits. According to BD results, the most important factor for aldolase binding to actin is the quaternary structure of aldolase and actin. Two pairs of adjacent aldolase subunits greatly add to the positive electrostatic potential of each other creating a region of attraction for the negatively charged subdomain 1 of the actin subunit that is exposed to solvent in the quaternary F-actin structure.

## INTRODUCTION

Actin microfilaments or F-actin (a polymer of G-actin) may play an important role in cellular metabolism by providing conditions for the high specificity of reactions within various metabolic pathways (Lakatos and Minton, 1991). Experimentally, many glycolytic enzymes bind cytoskeletal proteins reversibly; these include the muscle form of fructose-1,6-bisphosphate aldolase (aldolase), glyceraldehyde-3-phosphate dehydrogenase, 3-phosphoglycerate kinase, glucose phosphate isomerase, phosphofructokinase, pyruvate kinase, and lactate dehydrogenase (Knull and Walsh, 1992). These binding processes have been extensively studied in vivo and in vitro providing considerable physicochemical information regarding the interaction of glycolytic enzymes with G- and F-actin (Arnold and Pette, 1968; Magri et al., 1978; Walsh et al., 1980; Stewart et al., 1980; Walsh and Knull, 1988; O'Reilly and Clarke, 1993; Wang et al., 1996). Glycolytic enzymes bind F- and G-actin with different affinities, and binding is dependent on solution conditions such as pH, ionic strength, monovalent and divalent cations, and metabolite (ATP and ADP) (Arnold et al., 1971). The interaction between actin and aldolase is postulated to be electrostatic because the binding decreases with increasing ionic strength (Clarke and Masters, 1975; Walsh and Knull, 1988; Nakagawa and Nagayama, 1989). Studies have suggested that aldolase associates with G-actin at two different sites on the aldolase tetramer and that G-actin may be interacting with the active site of a subunit on one aldolase molecule and another G-actin interacts with a possible allosteric site on a second aldolase molecule to form a two G-actin/two aldolase complex (Magri et al., 1978).

During recent years, major efforts have been concerned with determining which amino acid residues are involved in the binding of glycolytic enzymes (especially aldolase) to F-actin. In 1993, O'Reilly and Clarke synthesized a peptide corresponding to the aldolase sequence 32–52 and observed that it competed with native aldolase for binding to F-actin. They concluded that one part of aldolase that is important for binding F-actin is among the residues 32–52 (O'Reilly and Clarke, 1993). In 1996, Wang and co-authors studied the catalytic activity and binding of aldolase mutants to F-actin. By mutating residues in and around the active site of aldolase to alanines, they found that Arg 42, Lys 107, and Arg 148 are important for the actin-binding activity (Wang et al., 1996). They also demonstrated that aldolase substrates such as fructose-1,6-bisphosphate, fructose-1-phosphate, and dihydroxyacetone phosphate reverse the gelling interaction of wild-type aldolase and F-actin (Wang et al., 1996). Thus, they concluded that there is partial overlap of catalytic site and actin-binding site in rabbit muscle aldolase (Wang et al., 1996). In 1996, Gustafson performed a comparison of the binding of glycolytic enzymes to yeast and rabbit muscle F-actin; she showed that the lack of binding of glycolytic enzymes to yeast actin as compared to the strong binding of glycolytic enzymes to rabbit muscle actin could be attributed to differences in a number of negative residues of the F-actin amino terminus (Gustafson, 1996). Furthermore, her site-directed mutagenesis experiments of F-actin suggested that the additional residues (24–25 and 99–100)

*Received for publication 10 April 1998 and in final form 25 September 1998.*

Address reprint requests to Dr. Kathryn A. Thomasson, Department of Chemistry, University of North Dakota, Grand Forks, ND 58202-9024. Tel.: 701-777-3199; Fax: 701-777-2331; E-mail: kathryn.thomasson@mail.chem.und.nodak.edu.



0006-3495/99/01/17/11 $2.00

may be important for aldolase binding to F-actin (Gustafson, 1996).

In this initial theoretical investigation, Brownian dynamics (BD) simulations of aldolase binding to F- or G-actin provide insights into which amino acids are important by applying simulations that are unbiased to particular residues. For example, are all residues suggested by experiments observed to interact simultaneously? Does only a subset interact, or are there other residues that have not yet been identified experimentally? BD may assist in interpreting site-directed mutagenesis experiments (e.g., what residue might be a candidate for mutation). These simulations may also provide a general orientation for the interacting proteins. Because aldolase interactions with actin are electrostatic (Clarke and Masters, 1975; Walsh and Knull, 1988; Nakagawa and Nagayama, 1989), coupling BD to rigorous numerical methods for computing electrostatics provides an excellent opportunity to gain information about the protein-protein interactions occurring with aldolase binding to G- or F-actin. Rather than a direct analysis of dynamics, BD is used as a powerful tool to generate a Boltzmann population of the protein-protein conformational states.

The BD method is well suited to the study of interacting biomolecules, such as protein-protein interactions. BD has been used for a decade to study the kinetics and energetics of rigid-body protein-protein association in complicated and realistic electrostatic fields. The main emphasis has been on calculating the bimolecular rate constants for protein-protein association (Northrup et al., 1988, 1993; Andrew et al., 1993; Gabdoulline and Wade, 1997). However, BD is capable of providing other information concerning macromolecular associations, including the prediction of the potential of mean force, estimation of the entropy of docking of protein pairs (Andrew et al., 1993), and the prediction of nonspecific encounter complexes between a protein and DNA (Thomasson et al., 1997). Our methods are generalized here for the first time to search for specific protein-protein interactions without biasing the reaction criterion for particular types of complexes.

Coupling BD to rigorous numerical methods for computing electrostatics provides an excellent opportunity to gain a quantitative understanding not only of the influences of the long-range electrostatic forces between a spatially complicated array of charges on two proteins, but also of the orientational aspects required for protein-protein association. Using the docking feature of BD, it is possible to identify the amino acid residues involved in complex formation, localize the regions of binding, and estimate the strength of binding between aldolase and G- or F-actin.

## COMPUTATIONAL METHODS

The program package MacroDox version 3.0.0 (Northrup et al., 1997) was used to assign the titratable charges on proteins, solve the linearized Poisson-Boltzmann equation, and run the various BD simulations; the BD algorithm for this package is detailed in Northrup et al. (1987) and overviewed along with the charge assignment and Poisson-Boltzmann algorithms in Northrup et al. (1993). It was necessary to resize arrays in this package to be able to handle the large multisubunit proteins, rabbit muscle aldolase and F-actin.

The x-ray structure of rabbit muscle aldolase, a tetrameric structure (the subunits are labeled A, B, C, and D as they appeared in the crystallographic coordinate file), was graciously provided by Nick Blom (Blom and Sygusch, 1997; Sygusch et al., 1987). The crystal structure for rabbit muscle G-actin (Kabsch et al., 1990) was obtained from the Brookhaven Protein Data Bank (Berstein et al., 1977), entry 1ATN. Residues 373–375, missing in G-actin crystal structure (Kabsch et al., 1990) were added using the coordinates from the model graciously provided by D. ben-Avraham (Tirion et al., 1995); the resulting G-actin structure was subjected to energy minimizations (50 steps of conjugate gradients with the AMBER force field (Weiner et al., 1984, 1986)) to resolve possible steric overlaps. The entire refined model was not used because it has been suggested that the refined models (Lorenz et al., 1993; Tirion et al., 1995) are inconsistent with the identification of rigid cores and flexible interdomain regions and are not representative of conformational changes upon actin polymerization (Page et al., 1998). The atomic model of F-actin was built from the structure of G-actin by subsequent rotations around helical axes ($Z$ axes) by $-166.14°$ and translations by 27.5 Å along the actin helix of the actin subunit according to the method and structural parameters given by Holmes et al., 1990; the model was a hexamer, with subunits labeled A, B, C, D, E, and F in order of how they were built into the helix. The F-actin hexamer model was also subjected to energy minimizations (200 steps of conjugate gradient minimization in the AMBER force field) to avoid the atomic overlaps between adjacent actin subunits. The minimization calculations in both cases were performed using Discover-3 module of Insight II 95.0 molecular modeling system (MSI, San Diego, CA). The united atom approach yielded heavy atom models of the proteins with 2936 atoms for G-actin, 17,616 atoms for F-actin hexamer, and 11,208 atoms for aldolase. Using the atomic coordinates of each model, the charges of titratable amino acids were assigned by applying the Tanford-Kirkwood method with static accessibility modification (Tanford and Kirkwood, 1957; Tanford and Roxby, 1972; Shire et al., 1974; Matthew, 1985) with the MacroDox charge set (Northrup et al., 1997) at pH 7.0, ionic strength of solvent 0.1 M, and a temperature of 298.15 K. The total charges of the proteins were as follows: G-actin, $-10.2e$; F-actin hexamer, $-54.4e$; and aldolase, $+16.8e$.

Following charge assignments, the electrostatic potentials (EP) about G-actin and aldolase were determined by numerically solving the linearized Poisson-Boltzmann (PB) equation on a cubic lattice by the Warwicker and Watson (1982) method with the adaptation of Klapper et al. (1986) as implemented in the program MacroDox (Northrup et al., 1997). The PB equation was solved on two cubic lattices with the center of mass (COM) of the molecule at the origin of lattice. The dimension of both grids was $81 \times 81 \times 81$, which is larger than the standard MacroDox grid. The resolution of the inner grid was 1.8 Å, providing a grid large enough to enclose the edges of the molecules with at least 5 Å to spare. The outer grid was three times coarser (5.4 Å) and contained the values of potentials at distant regions around the molecule. These two values of grid resolutions were a compromise between the size of the molecules and the intention to keep the details of electrostatic potential on an atomic scale. The molecular surfaces of the proteins were defined as the point of contact between a sphere with a radius of a water molecule (1.4 Å) and the molecular van der Waals surface. The spaces enclosed by the molecular surfaces, or the interior regions, were assigned a low dielectric constant of 4 and zero value of ionic strength. Exterior regions outside the molecular surfaces were assigned a high dielectric constant, 78.3. The pattern of electrostatic potential about the molecules was visualized using the contour utility and the viewer module of the Insight II 95.0 molecular modeling system (MSI).

Next, BD simulations of G-actin binding to aldolase were performed to identify the formation of complexes. For the simulation of interactions between aldolase and G-actin, 10,000 trajectories were run taking almost 141 CPU hours on an SGI INDY R4400 175-MHz workstation. At the beginning of each trajectory, the COM of G-actin was placed on the surface of a sphere of radius 102 Å from the COM of aldolase, and the angular position and the orientation of G-actin were chosen randomly. Both mol-

ecules were allowed to rotate and translate. When the COM of G-actin reached the surface of a sphere 250 Å from the COM of aldolase, the trajectory was terminated. To prevent steric overlap between molecules during a simulation, a 1-Å exclusion grid (size 111 × 111 × 111, larger than standard MacroDox arrays) was built around aldolase. When the COMs of the proteins were close to each other, before accepting a translational or rotational Brownian step, each surface atom of G-actin was checked against the aldolase exclusion grid; Brownian steps placing an atom in occupied grid cells were rejected. The time step of the displacement and rotation varied based on the distance between the COMs of interacting molecules; the time step was smaller when proteins were close together. During the simulation, the structure of each complex was stored for each trajectory for which the value of electrostatic energy of G-actin in a field of aldolase was lowest. If the value of the electrostatic interaction energy for a given trajectory was less than $-8kT$, the corresponding structure was saved for subsequent analysis.

For the simulation with F-actin, the electrostatic potential calculation was determined as follows. Using the model of an F-actin hexamer, the origin of the coordinate system was placed at the COM of the hexamer. The $z$ axis of the coordinate system almost coincided with the helical axis of F-actin and was parallel to it. The electrostatic potential of the entire hexamer was calculated with an outer grid of size 4.125 Å and an inner grid of size 1.375 Å. The dimensions of both grids (81 × 81 × 81), the method of solution of the Poisson-Boltzmann equation, and the procedure of assigning the value of dielectric constant at grid points were the same as those applied to the EP calculation of G-actin and aldolase. The overall size of inner grid was 110 Å; it covered the central part of the hexamer and contained 11,739 atoms of the total 17,616 atoms. Thus, there were hexamer atoms outside of the inner grid (with absolute value of $Z$ coordinate more than 55 Å). The outer grid was used to create the boundary condition on the top and the bottom faces of the inner grid so that, essentially, the EP calculated approximated the EP of an infinite actin filament within the region of space defined by the inner grid.

To simulate binding to F-actin, aldolase was allowed to diffuse (i.e., rotate and translate) within a truncated cylinder around the F-actin filament (which was not allowed to move); the cylinder was constructed with the same height (110 Å) as the inner grid solution of the Poisson-Boltzmann equation described above. The periodic property of the filamental structure was used for the calculation of the electrostatic forces acting on aldolase atoms; when aldolase moved too far along the $z$ axis to take it outside the inner region, it was repositioned back into the cylinder. Initially, the COM of aldolase was positioned in an equatorial plane that crosses the middle of the actin hexamer ($Z = 0$) 150 Å from the helical axis and at random orientations. In the course of the simulation, if the COM of aldolase moved along the $z$ axis farther than +55 Å, the whole aldolase molecule was shifted by −27.5 Å and rotated by angle 166.14° around the actin helix; similarly, if it moved farther than −55 Å, the transformation was a translation of +27.5 Å and a rotation of −166.14°. Such transformations corresponded to the helical parameters of F-actin so that aldolase was placed in the same conformation regarding the F-actin helix. Thus, aldolase movement was limited to a cylinder (positioned at $-55$ Å $< Z <$ 55 Å from bottom to top) corresponding to four internal subunits of an actin helix, while mimicking an infinite actin helix and avoiding the ends of the F-actin hexamer. Moreover, while calculating the electrostatic forces between aldolase and F-actin or while checking the overlaps between aldolase atoms and the F-actin exclusion grid (built around the F-actin hexamer the same way as around aldolase for BD of G-actin and aldolase) a similar temporary shift was applied when necessary. This allowed all aldolase atoms to be treated as if they were inside the cylinder. During a trajectory, if the distance between the COM of aldolase and the F-actin helix reached 200 Å, aldolase was relocated to a position 150 Å from the helix axis while maintaining the same orientation. Thus, the simulation forced aldolase to spend more time in a region close to F-actin. Each individual trajectory was terminated when aldolase performed 200,000 BD steps with a distance between the aldolase COM and F-actin helix less than 120 Å. As in case of the G-actin/aldolase simulation, the most stable complex in course of a trajectory was saved if its electrostatic interaction energy was less than $-8kT$. 900 BD trajectories took 240 h of CPU time on the 175-MHz SGI Indy R4400.

In addition to visual examination of the structure of saved complexes, the statistical analysis was performed using MacroDox. The statistical analysis determined the number of occurrences that each charged amino acid formed intermolecular contacts between proteins in the revealed complexes.

## RESULTS

The pattern of the EP around a protein is determined predominantly by the charged amino acid residues that are located on the surface. Areas of the molecular surface with high content of charged residues with the same sign supply an EP that extends considerable distances from the surface of the protein. Such areas can be considered as most favorable regions for binding. Surface regions that include charged residues of both signs generate EPs that are highly spatially inhomogeneous whereas others show high concentration of a specific charge. We have identified the broad regions of strong electric potential for each protein.

### Aldolase

There are two broad regions of strong positive potential around aldolase (Fig. 1); the first is between subunits A and D, and second is between subunits B and C. These regions are a result of the quaternary structure of aldolase where two adjacent subunits (A and D or B and C) form a groove. The grooves are located on opposite sides of the tetramer and are slightly extended in one direction (Fig. 1). Within a groove,

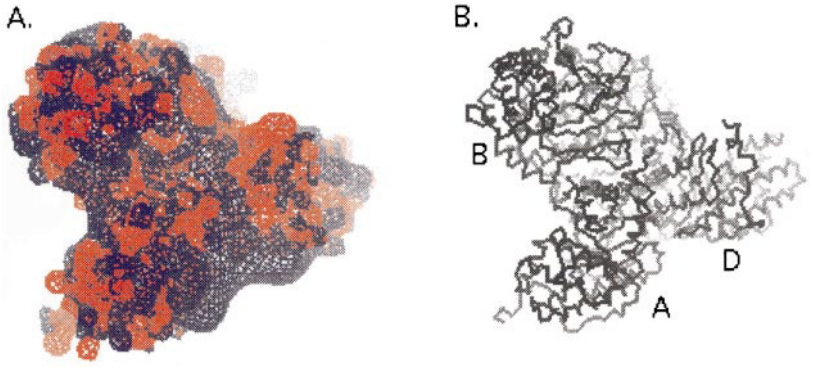


FIGURE 1 (*A*) The electrostatic potential for rabbit aldolase. The red contours represent an isopotential surface where charge 1*e* possesses electrostatic energy equal to −0.5 kcal/mol; the blue isopotential surfaces are for energy +0.5 kcal/mol. The groove between A and D subunits of aldolase is located in lower right corner of the picture, is blue in color, and represents a positively charged surface. (*B*) The trace presentation (only $C^{\alpha}$ atoms) of aldolase structure. Subunits A, B, and D are labeled. The subunit C is located behind the plane of the figure behind subunit B.

there are four arginines at the bottom, Arg 257 and 258 (two from each adjacent subunit). The groove walls are covered by positively charged residues from each subunit: Lys 12 and 13, Arg 21, and Lys 27, 341, 288, and 293. There are no negatively charged residues inside these grooves. The lack of negatively charged residues in the groove and the side chain conformation of the groove residues brings the high density of positive charge and, hence, the homogeneous region of strong positive potential. Moreover, the Lys 288, 293, and 341 form a triangle on each subunit's surface (the distance between the NZ (epsilon amino nitrogen) atoms of Lys 288 and Lys 341 = 9.47 Å, of Lys 341 and Lys 293 = 13.75 Å, and of Lys 293 and Lys 288 = 9.49 Å), creating two additional regions of strong positive surface potential. Other regions of the aldolase surface demonstrate the alternating pattern of positive and negative EP caused by surface charges of different signs.

## G-actin

According to the classification of Kabsch et al., 1990, the actin molecule can be schematically subdivided into four subdomains: subdomain 1 (residues 1–32, 70–144, and 338–375), subdomain 2 (residues 32–69), subdomain 3 (residues 145–180 and 270–337), and subdomain 4 (residues 181–269). Subdomain 1 is covered by a homogeneous cloud of negative potential (Fig. 2, lower right corner). This strong negative potential is supplied by a large number of negatively charged residues (Asp 1, Glu 2, Asp 3, Glu 4, Asp 24 and 25, Glu 99 and 100, Tyr 133 and 143, Glu 361, Tyr 362, Asp 363, and Glu 364) located on the molecular surface; there is only one positively charged Lys 359 in subdomain 1. The Arg 28 and 95 are located at the border of the negative potential of subdomain 1. The EP around subdomain 2 (upper right corner of Fig. 2) presents the sequence of positive and negative islands that is quite inhomogeneous. Subdomain 3 (Fig. 2, lower left corner) is covered by positive potential with small negative patches. The EP around the subdomain 4 (Fig. 2, upper left quadrant) can be described as a central hemisphere of positive potential, caused by the cluster of residues Lys 191, Arg 196, Lys 238, and Arg 254 and 256, surrounded by a ring of negative potential from residues Asp 187, Tyr 188, Glu 195, Tyr 198, Glu 205 and 207, Tyr 218, Asp 222, Glu 224, 226, 237, and 241, Asp 244, Glu 259, and Tyr 306. Briefly speaking, there are two broad areas of predominantly negative potential, the first around subdomain 1 and the second around the subdomain 4. These regions are located on opposite sides of the actin globule.

## F-actin

Because the F-actin helix is formed by the interaction of G-actin molecules (Holmes et al., 1990), much of the G-actin surface is not available for creating interactions with proteins other than itself. Subdomain 4, for example, is involved in intersubunit contacts within the F-actin helix, and its negative potential is greatly reduced because of the positive potential of nearby subunits. Subdomain 1, on the other hand, bears a strong negative potential located at the outer radii (where the helix is the widest) of the F-actin helix (Fig. 3). Subdomain 1 is fully accessible to solvent and almost does not feel the charges from neighboring subunits. From the point of view of the EP, F-actin can be seen as a double helix of bulbs of negative potential extending into the solvent separated by regions of variable signs located close to the helical axis. Thus, the subdomain 1 of each actin subunit can be considered as a viable candidate for aldolase binding.

## BD-identified G-actin/aldolase complexes

The 10,000 BD trajectories of G-actin with aldolase gave 1356 complexes with electrostatic energy less than $-8kT$. The distribution for the G-actin COMs for all complexes around aldolase is presented in Figure 4 *A*. The majority of these complexes have the G-actin COM located in the region of space between aldolase subunits B and C or between A and D. Thus, stable complexes between aldolase and G-actin are formed when G-actin binds to the positively charged grooves of aldolase. There are a few complexes for which the G-actin COM is located either between A and B or between C and D subunits; however, the number of such

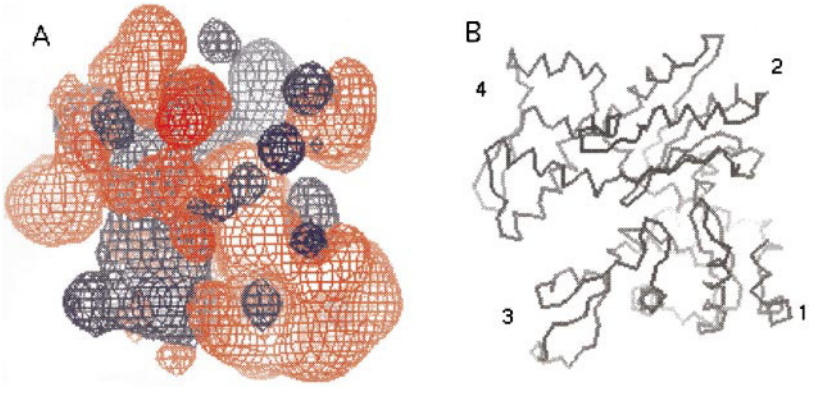


FIGURE 2 (*A*) The electrostatic potential for G-actin. The red contours represents isopotential surfaces where charge 1*e* possesses electrostatic energy equal to −0.5 kcal/mol; the blue isopotential surfaces are for energy +0.5 kcal/mol. The G-actin molecule is oriented so that subdomain 1 is shown in the lower right corner (showing a red bulb of negative potential) and subdomain 4 is in the upper left corner showing a red ring of negative potential surrounding a blue (positive) center. (*B*) The trace presentation (only $C^{\alpha}$ atoms) for the structure of G-actin. The subdomains 1, 2, 3, and 4 are labeled.

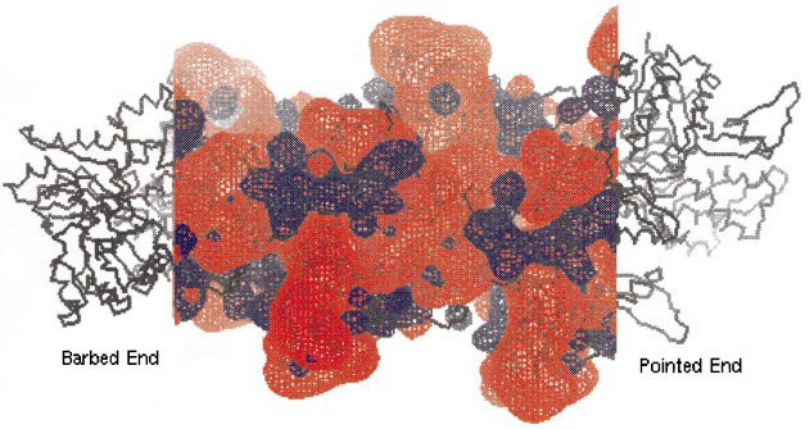


FIGURE 3 The electrostatic potential for F-actin hexamer central part. The red contours represent an isopotential surfaces where charge 1*e* possesses electrostatic energy equal to −0.5 kcal/mol; the blue isopotential surfaces are for energy 0.5 kcal/mol. The trace presentation (only $C^{\alpha}$ atoms) for the structure of F-actin hexamer is shown in black. The helical axis of the hexamer is located horizontally through the center of the protein. The pointed and barbed ends of the hexamer are labeled. There are four red negative regions directed outside the helical axis that correspond to the negative electrostatic potential around subdomain 1 of each actin subunit in a central part of the hexamer.

complexes is significantly smaller than the number of complexes where G-actin is bound to one of the two positive grooves of aldolase. Fig. 4 *B* presents the distribution of aldolase COMs around G-actin. For the majority of the complexes, the aldolase COM is located in the vicinity of subdomain 1 of G-actin (lower right part of molecule in Fig. 4 *B*). These complexes represent G-actin binding to aldolase at subdomain 1. Fig. 4 *B* also shows complexes where the aldolase COM is located around subdomain 4 (higher left quadrant of molecule in Fig. 4 *B*). Although the number of such complexes is much smaller than the number of complexes where G-actin is bound by subdomain 1, the common feature of both these subdomains is the negative EP. From these two figures we can conclude that the dominant binding region of G-actin to aldolase is determined by the attraction of G-actin by one of its negatively charged subdomains to the one of positively charged grooves of aldolase.

This conclusion is supported by determining the frequency of occurrence of each amino acid involved in intermolecular contacts shorter than 6 Å (Fig. 5, *A* and *B*). It is the residues of the G-actin amino terminus (Asp 1 and Glu 2 and 4), the carboxy terminus (Glu 364, Asp 363, and Lys 359) and Glu 125, 99, and 224 that are frequently involved in complex formation (Fig. 5 *A*). All these residues belong to subdomain 1 of an actin subunit. Aldolase lysines from the positively charged triangle, Lys 341 and 293 and, to a lesser degree, Lys 293 are most frequently involved in intermolecular contacts (Fig. 5 *B*). From a structural perspective, these data show that the binding of G-actin subdomain 1 to one of the two positively charged grooves of

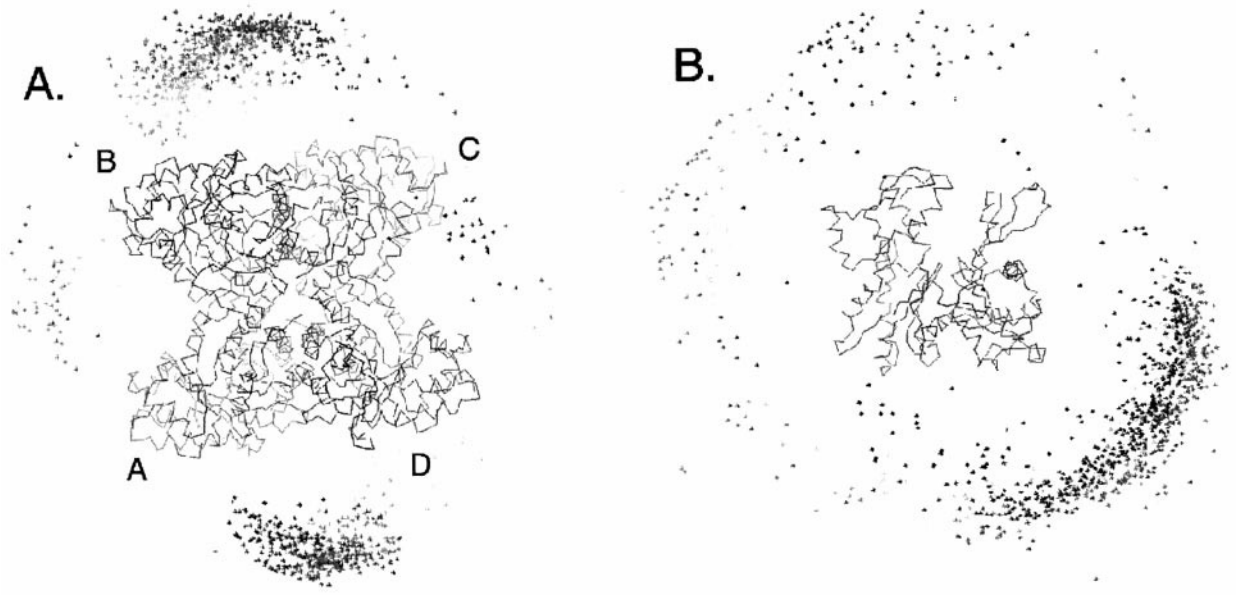


FIGURE 4 (*A*) Distribution of G-actin COM around aldolase. The aldolase molecule is represented as a $C^{\alpha}$ trace. Each dot represents the center of mass of a G-actin in an encounter snapshot with aldolase. Note that the two predominant regions of aldolase to which actin binds are the groove regions of positive potential between the aldolase subunits (Fig. 1). (*B*) Distribution of aldolase COM around G-actin. The distribution of complexes presented are the same as those in Fig. 4 *A* but are presented here from the perspective of G-actin. G-actin is represented as a $C^{\alpha}$ trace. Each dot represents the center of mass of an aldolase in an encounter snapshot with G-actin. Note the two predominant regions of G-actin to which aldolase binds; these include subdomain 1 and subdomain 4 of G-actin.

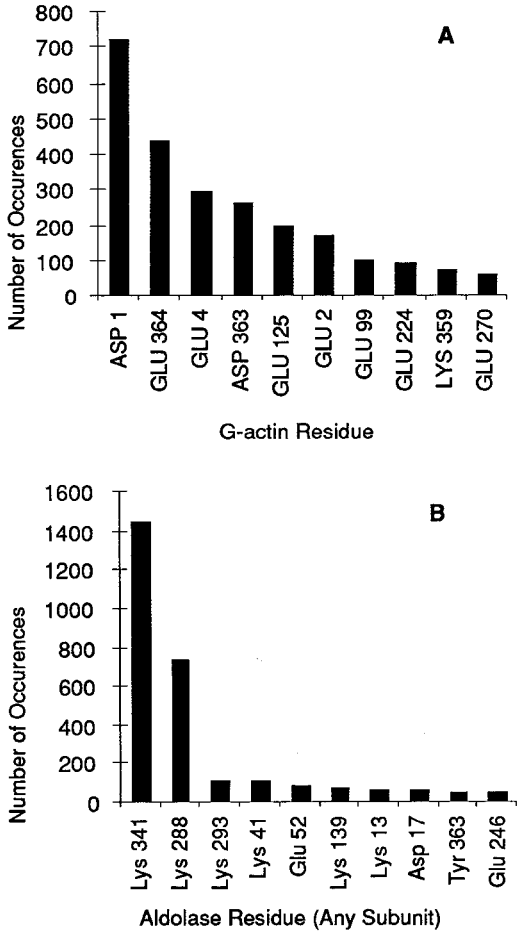


FIGURE 5 (*A*) The number of occurrences of G-actin amino acid residues in complexes with aldolase (contacts shorter than 6.0 Å are counted). (*B*) The number of occurrences of aldolase amino acid residues (any subunit) in complexes with G-actin (contacts shorter than 6.0 Å are counted).

aldolase is the dominant binding mode between globular actin and aldolase.

The first 200 most stable complexes between G-actin and aldolase (spanning the energy range from −13.6 up to −9.5 kcal/mol) were analyzed. There are two types of complexes, type I and type II, both of which bind to subdomain 1 of G-actin. There are 174 type I complexes, and there are 26 complexes of type II, which are the more electrostatically stable. The intimate salt bridges between the most stable example of each complex type are presented in Table 1.

For complexes of type I, the most intimate salt bridges (typically 2–3 Å) are formed by the positively charged nitrogens from Lys of aldolase (Lys 341, 288, 293, 13, and 41) and negatively charged oxygens from Glu or Asp of subdomain 1 of actin (amino-terminal residues 1, 4, and 2; carboxyl-terminal residues 363 and 364; and Glu 125 and 99) (Fig. 6). For a majority of these complexes, the intimate first salt bridge is complemented by an attraction between a second and third pair with distances around 3–6 Å. This Coulombic interaction between additional pairs of oppositely charged atoms contributes significantly to the stability of the complex. From data presented in Fig. 4, the most frequent kind of complex observed is type I. For such complexes, the G-actin is bound by its subdomain 1 to one of the positively charged aldolase grooves. This preference in binding can be explained by the parts of molecules that generate the strong homogeneous electrostatic potential of opposite sign. Attraction between them is strong and can steer as they approach each other in solution. Formation of type II complexes requires a finer sterical tuning and a specific orientation, so they are less favorable from an entropic perspective even if more electrostatically stable.

Complexes of type II (unlike the more common type I) were formed by the interaction of negatively charged surface residues of aldolase with the positively charged residues of G-actin. One of the negative spots on the aldolase surface is located between subunits A and B and includes Glu 52 and 81 from subunits A and B (Table 1). G-actin forms a salt bridge with Lys 359 of subdomain 1 to residues in the groove between A and B of aldolase. Additional stabilization of these complexes is achieved by a second salt bridge between actin Glu 364 and Lys 110 or 139 of aldolase subunits A or B.

## BD-identified F-actin/aldolase complexes

The 900 BD trajectories of aldolase with F-actin gave 764 complexes. The statistical analysis revealed the number of occurrences of amino acids in intermolecular contacts shorter than 6.0 Å (Fig. 7). Residues most frequently involved in complex formation are almost the same as those in the case of G-actin/aldolase; for aldolase, the residues are from the positively charged triangle (Lys 341, 288, and 293), and for F-actin, the residues are from subdomain 1. Therefore, the binding mode of aldolase to actin filaments should be almost identical with the binding mode of G-actin to aldolase. Analysis of the 200 most stable complexes between aldolase and actin filaments showed that they could be divided into two classes. Class I comprised complexes where aldolase forms the close contacts with just one actin subunit (there were 135 such complexes from a total of 200; Fig. 8). Class II comprised complexes where aldolase is bound to two adjacent subunits in the same strand of F-actin (Fig. 9).

The overall structure of class I complexes was identical to type I complexes between G-actin and aldolase. The only difference is the value of the electrostatic energy between the proteins; the electrostatic energy was lower for aldolase/F-actin interactions because aldolase experiences not only the EP of the particular actin subunit to which it is bound but also the EP of neighboring actin subunits. The energy of the most stable complex where aldolase bound to one actin subunit was equal to −15.0 kcal/mol. As in a case of G-actin/aldolase complexes of type I, the acidic residues from subdomain 1 of an actin subunit (amino terminus, carboxy terminus, and surface aspartates and glutamates)

**TABLE 1 Most intimate salt bridges identified in complexes of aldolase with G-actin**

| | | | Aldolase | | G-actin | |
|---|---|---|---|---|---|---|
| Complex Type | Energy (kcal/mol) | Distance (Å) | Residue | Atom | Residue | Atom |
| I | −11.19 | 1.92 | Lys 288D | NZ | Asp 1 | OD2 |
| | | 4.73 | Lys 341A | NZ | Glu 125 | OE2 |
| | | 5.58 | Lys 341D | NZ | Glu 2 | OE1 |
| | | 5.87 | Lys 288D | NZ | Asp 1 | NT |
| | | 5.87 | Lys 288A | NZ | Asp 363 | OD1 |
| | | 6.00 | Lys 341A | NZ | Asp 363 | OD1 |
| | | 6.01 | Lys 341D | NZ | Asp 1 | NT |
| | | 6.01 | Lys 288D | NZ | Glu 4 | OE1 |
| II | −13.56 | 1.94 | Glu 52B | OE2 | Lys 359 | NZ |
| | | 2.97 | Glu 52B | OE1 | Lys 359 | NZ |
| | | 3.73 | Glu 52A | OE2 | Lys 113 | NZ |
| | | 4.43 | Glu 52A | OE1 | Lys 113 | NZ |
| | | 4.75 | Glu 81B | OE1 | Lys 359 | NZ |
| | | 5.09 | Lys 110B | NZ | Glu 364 | OE1 |
| | | 5.44 | Glu 81B | OE2 | Lys 359 | NZ |

Energy is the electrostatic energy of G-actin in the electric field of aldolase. Distance is that between atoms; residue names, residue numbers with subunit identification, and the atom names are as defined in the crystal structure file.

form salt bridges with lysines located in one of the two groove regions of aldolase. Although the patterns of intermolecular salt bridges for complexes may vary, the overall picture of aldolase binding to actin filaments is the same; aldolase binds to the negatively charged external part of the actin helix, subdomain 1 of the actin subunit (Fig. 8). The actin residues involved include Glu 2, Asp 1, Glu 4, Asp 363, Glu 99, 125, and 364 (Fig. 7 *A*). These residues are fully accessible from solution and generate a homogeneous negative potential (Fig. 3). The residues that belong to subdomain 4, which also generate negative EP and demonstrate binding ability to aldolase, are not exposed to the surface when actin polymerizes to form filaments, and the pattern of the electric field generated by subdomain 4 is greatly affected by the electric field from neighboring actin subunits. Aldolase residues identified as important for binding the subdomain 1 of actin are Lys 341, 288, and 293 (Figure 7 *B*). As mentioned previously, these three lysines on each aldolase subunit generate the strong positive potential and contribute the most to the formation of complexes. Other aldolase residues involved in complex formation are located close to this triangle, and their ability to participate in binding depends on the overall orientation of the aldolase tetramer regarding actin helix. The shape of actin subunit subdomain 1 and the shape of positive grooves (the groove between subunits B and C is shown in this figure) are complementary to each other (Fig. 8). The contact surface area for such complexes varies from complex to complex and is $\sim 200 \pm 20$ Å$^2$.

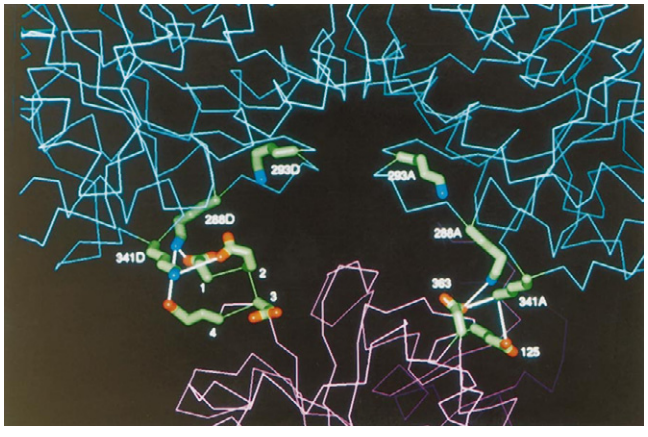


FIGURE 6 Interaction region of a single complex of aldolase with G-actin. An enlargement is shown of the close contact region for complex II (Table 1) between aldolase (cyan) and G-actin (pink). The interaction region on aldolase is the groove between subunits A and D. The interaction region on G-actin is subdomain 1.

As mentioned above, the overall geometry of the complexes between aldolase and one of the internal actin subunits in a filament is very similar to the geometry of type I G-actin/aldolase complexes because the same actin domain is involved. Among the 200 most stable aldolase/actin filament complexes, there were no type II G-actin/aldolase complexes. Such binding is not possible because of steric overlaps of aldolase atoms with an actin subunit on an opposite strand of the helix.

Class II complexes between aldolase and actin filaments occur where aldolase forms contacts with two adjacent subunits in a particular strand of the actin helix (Fig. 9). Such complexes are relatively rare (65 of 200) and less stable (the most stable electrostatic interaction energy was −13.3 kcal/mol) as compared with complexes where aldolase binds to only one subunit. In class II complexes, aldolase is rotated about an axis perpendicular to the actin helix by an angle that allows it to make the close contacts with two adjacent actin subunits. Such rotations allow for contacts between the aldolase positive groove and subdomain 1 of one actin subunit and also create salt bridges between residues of subdomain 1 of a neighboring actin subunit and one of the aldolase residues Lys 139, 316, 317, and 321. For

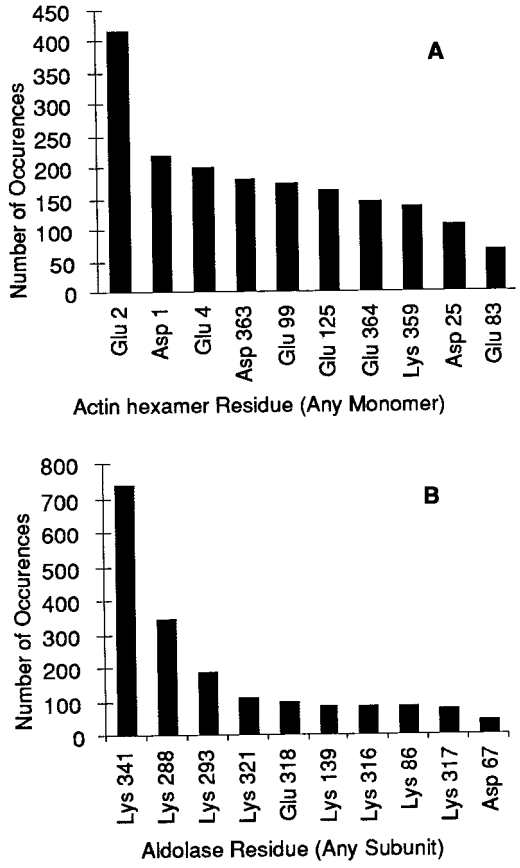


FIGURE 7 (*A*) The number of occurrences of F-actin amino acid residues (any subunit) in complexes with aldolase (contacts shorter than 6.0 Å are counted). (*B*) The number of occurrences of aldolase amino acid residues (any subunit) in complexes with F-actin (contacts shorter than 6.0 Å are counted).

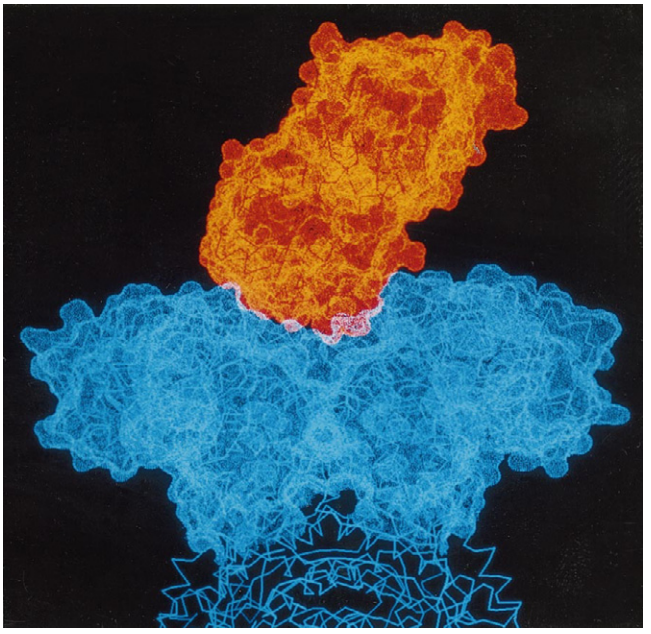

FIGURE 8 Connolly surface of the most common complex of F-actin with aldolase (class I). The surface includes subunits B and C of aldolase and one subunit of F-actin (second in the hexamer). F-actin is oriented so that the view is directly down the actin helix. Please note that the picture for the most common class of complexes of aldolase with G-actin shows the same geometry.

example, in the most stable class II complex (Fig. 9), there are three salt bridges: 1) actin Glu 2D, OE2 (a γ-carbonyl group), and aldolase Lys 341D, NZ (distance, 2.97 Å); 2) actin Glu 125D, OE1, and aldolase Lys 341A, NZ (distance, 3.97 Å); and 3) actin Glu 361F, OE2, and aldolase Lys 139A, NZ (distance, 2.88 Å). The first two salt bridges are between atoms of actin subunit D and the aldolase positive groove between subunits A and D. The third salt bridge is between actin subunit F and an aldolase Lys that does not belong to the positive groove between subunits A and D. The wide regions of homogeneous EP around actin subdomain 1 and the positive grooves of aldolase make possible slight changes in the orientation of aldolase so that the formation of intermolecular contacts between neighboring actin subunits is possible.

## DISCUSSION

The BD simulation of the interaction of aldolase with G- or F-actin revealed two unique complexes between the proteins. In the first, the positively charged grooves on the surface of aldolase, formed between subunits A/D or B/C, bound to subdomain 4 of actin. This pattern is possible only for interaction with G-actin because subdomain 4 is masked in F-actin. In the second, a more universal binding scheme results from the electrostatic attraction of the positively charged grooves on aldolase with the homogeneously negative subdomain 1 of actin whether in the monomeric G-

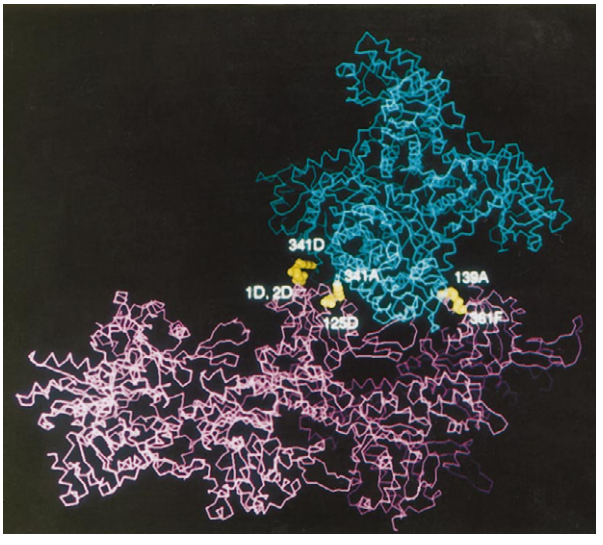


FIGURE 9 Structure of an example of a class II complex of aldolase with F-actin. The $C^{\alpha}$ trace of aldolase is cyan, and the $C^{\alpha}$ trace of an actin hexamer is pink. The contacting amino acid residues from both proteins are shown in yellow and labeled. Aldolase forms three close contacts with two adjacent actin subunits.

actin state or in the polymeric F-actin state. It is clear from our study that native multimeric proteins should be used in these kinds of investigations because simply using a subunit or a piece of a subunit may not identify the native binding domains. As mentioned previously, the neighboring aldolase subunits A/D or B/C generate a cluster of positively charged residues. The helical structure of F-actin produces the bulbs of homogeneous negative potential. The Coulombic attraction between the positive groove on aldolase and the negative bulb on F-actin results in sufficient energy to permit binding.

Mutant studies (Gustafson, 1996) where the actin residues (Asp 24–25, Glu 99–100, Asp 80–81, Glu 83, and Lys 84) were converted to alanines have shown that the mutation of the first two pairs (Asp 24–25 or Glu 99–100) increases the dissociation constant of F-actin/aldolase complex compared with wild type 4.5 and 3.4 times, respectively (Gustafson, 1996). Mutation of Asp 80–81 brings less than two times the increase in the dissociation constant (Gustafson, 1996). The BD-identified complexes agree qualitatively that the most frequent residues in the F-actin/aldolase complexes involve Asp 24–25 and Glu 99–100 the most and Asp 80–81 the least. Moreover, the BD results suggest other actin residues (for example, Glu 2, 4, 125, and 364 and Asp 1 and 363) for which mutations may show the increase in a dissociation constant of the complex.

O'Reilly and Clarke in 1993 identified one actin-binding site on aldolase to be located within residues 1–164. BD also identified several residues in this region, including Lys 139, 86, and 13, Asp 67, Glu 49, and Arg 91, as important, but the most common BD-identified residues do not fall in this region. O'Reilly and Clarke, however, demonstrated that a synthetic peptide corresponding to the region of aldolase that contains sequence motif aldolase 32–52 was capable of competing with aldolase for binding to actin filaments (O'Reilly and Clarke, 1993). This peptide contains two positively charged residues in the middle, Lys 41 and Arg 42, which would be attracted to negative F-actin so that competitive binding is possible; however, a single peptide cannot represent all the possible electrostatic interactions that result from the tertiary or quaternary structure of the intact protein. The BD results do not show any sufficient participation of aldolase residues 32–52 because this peptide when taken as part of the overall quaternary structure does not generate a large enough region of positive potential as do the grooves that formed between adjacent subunits. The most important factor for aldolase binding to actin is the quaternary structure of the aldolase molecule. Two pairs of adjacent aldolase subunits greatly enhance the positive electrostatic potential of each other, creating a region of attraction for negatively charged surface patches from other molecules. It may be possible for BD to identify interactions of a peptide with the same sequence as aldolase 32–52 when the entire quaternary structure of aldolase is not included in the simulation; preliminary results of BD simulations of this peptide interacting with F-actin currently underway in our laboratory indicate that the peptide binds.

BD results assume that only solvent-accessible charged aldolase residues participate in complex formation with actin. Residues from the active site of aldolase (Arg 42, Lys 107, and Arg 148) are able to reach the surface of the protein but because of the quaternary structure of aldolase are inaccessible to large structures such as monomeric or polymeric actin. Wang et al. (1996) used site-directed mutagenesis studies to show that aldolase residues near the active site (Arg 42, Lys 107, and Arg 148) appear to be necessary for catalytic activity and for the normal actin-binding activity because each mutation significantly reduced actin binding. The current BD studies show no evidence of this because the regions in question are buried inside the quaternary structure of aldolase. Although they are near the surface, large structures such as actin cannot access it; a small substrate could still access the active site. It is possible that a substantial conformational change of the aldolase after initial association could expose residues in the region of the active site for interaction with F-actin. Because BD treated each protein as a rigid rotor, flexibility of the proteins after binding was not included in the simulations; to include protein flexibility may bring BD predictions into better accordance with observations of Wang et al., 1996. Furthermore, the crystal structure does not include the coordinates of the substrate so that it is not yet possible to test for differences in binding of aldolase plus substrate with F-actin.

Taking 13 actin subunits (a full period of the actin helix as described by Holmes et al., 1990) and placing aldolase in the class I complex conformation on every actin subunit that does not cause steric clashes with an aldolase on a nearby actin subunit, we estimate that 13 actin subunits can bind up to seven molecules of aldolase. The schematic view of this binding is presented in Fig. 10.

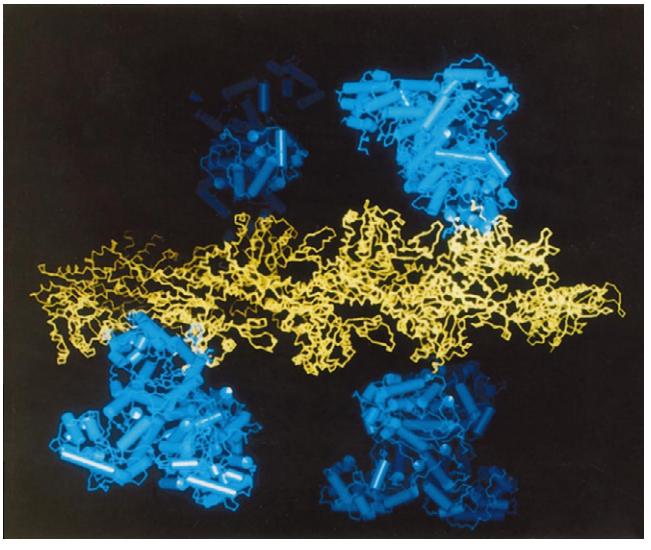

FIGURE 10 The schematic presentation of saturated binding of aldolase to F-actin. The F-actin (yellow) is located in the center with a horizontal helical axis. The backbones of nine actin subunits are shown. Four aldolase tetramers appear in secondary rendering (blue).

The present study has a few shortcomings. First, we assumed the predominance of Coulombic electrostatic forces and have not considered hydrophobic effects. This, however, is reasonable as the binding of aldolase to actin has been shown to be predominantly electrostatic (Clarke and Masters, 1975; Walsh and Knull, 1988; Nakagawa and Nagayama, 1989). Hydrophobic forces would begin to play a more important role in the creation of extremely intimate complexes and would be critical to the prediction of realistic binding constants. Second, we do not include the flexibility the proteins during the simulations. For example, the amino terminus of actin, which we have identified as important to binding aldolase, can shift within an actin subunit. What supports our findings is the experimental evidence (Gustafson, 1996) that it is the amino-terminal region of F-actin that is critical to binding aldolase. Thus, even if the amino terminus of F-actin shifts within the actin helix, it must still be located on the surface of the actin helix so that it may interact with aldolase. The complexes we identify repeatedly indicate the same residues as being important for binding, but these complexes should not be considered a lowest energy optimum for a single most intimate complex; all complexes we identify could be made more intimate by applying traditional molecular dynamics, but as our primary goal was to determine what parts of actin and aldolase are critical for binding, predicting a single most intimate complex is not necessary. Finally, we did not include explicit cations in either the high-affinity site or the low-affinity cation-binding sites of G-actin. The high-affinity site is located close to the binding site of ATP and is positioned nearly at the center of the G-actin globule (Kabsch et al., 1990). Therefore, the inclusion of either ATP or the $Ca^{2+}$ ion in the model will not appreciably change the electric field predicted around the subdomains 1 or 4 of the actin subunit and, hence, the binding mode of aldolase. The location of the low-affinity sites are still unknown so that it is not yet possible to include them in the models of G- or F-actin; however, the low-affinity sites have been shown to be important for polymerization of F-actin (Carlier, 1991); DalleDonne et al. (1997) have shown that an actin subunit binds five $Ca^{2+}$ ions at low-affinity sites. These sites can significantly reduce the net charge of an actin subunit, which would explain why G-actin binds aldolase only at low ionic strengths (Magri et al., 1978) when these sites would not be occupied. Despite the lack of bound cations, the current and simulations do show that at $I = 0.01$ M and 0.1 M the same complexes are uncovered; the major difference is that the aldolase spends more time in the vicinity of the actin molecule at the lower ionic strength. Basically, the complexes identified in this BD study can be considered the kinds of complexes that would be found at low ionic strength. Concerning F-actin, as we are not considering actin polymerization and because aldolase has been shown to have a high affinity for F-actin, even under higher ionic strengths (aldolase actually has a higher affinity for F-actin than for G-actin (Gustafson, 1996)), the occupancy of the low-affinity sites may be more important for the polymerization of actin and not important for the polymeric F-actin binding of aldolase that has been considered here.

Finally, the major finding of the BD simulations is that the quaternary structure of the proteins are crucial for identifying the patterns of binding. The positively charged groove formed between two subunits of aldolase interact with the negatively charged subdomain 1 of F-actin. Now that the patterns of aldolase binding to G- and F-actin have been identified, future studies will include using this specific information as reaction criteria for the prediction of rate constants. To predict rate constants for the association of two proteins, specific docking criteria are required (Gabdoulline and Wade, 1997). The current BD study with aldolase and actin has pioneered the use of a general docking criterion to identify more specific regions of the proteins that may possibly be used to create specific docking criteria. Our future studies will incorporate specific docking criteria and provide more statistical data including thermodynamic and kinetic parameters in binding of aldolase to actin such as the mean free energy of binding and the association and dissociation rate constants. We will also continue exploring the effect of actin mutants, ionic strength, and pH on simulated results.

We thank Dr. Nick Blom of Universite de Montreal for providing x-ray coordinates of rabbit aldolase, Dr. D. ben-Avraham from Clarkson University for sending us the coordinates of the refined F-actin model, and Prof. Scott Northrup of Tennessee Tech for assistance with the MacroDox3.0 package.

This research was funded by grants from the National Institutes of Health and North Dakota EPSCoR.

## REFERENCES

Andrew, S., K. A. Thomasson, and S. H. Northrup. 1993. Simulation of electron-transfer self-exchange in cytochromes c and $b_5$. *J. Am. Chem. Soc.* 115:5516–5521.

Arnold, H., R. Henning, and D. Pette. 1971. Quantitative comparison of the binding of various glycolytic enzymes to F-actin and the interaction of aldolase with G-actin. *Eur. J. Biochem.* 22:121–126.

Arnold, H, and D. Pette. 1968. Binding of glycolytic enzymes to structure proteins of muscle. *Eur. J. Biochem.* 6:163–171.

Berstein, F. C., T. F. Koetzle, G. J. B. Williams, E. F. Meyer, Jr., M. D. Brice, J. R. Rodgers. O. Kennard, T. Shimanouchi, and M. Tasumi. 1977. The protein data bank: a computer-based archival file for macromolecular structures. *J. Mol. Biol.* 112:535–542.

Blom, N., and J. Sygusch. 1997. Product binding and role of the C-terminal region in class 1 D-fructose 1,6-bisphosphate aldolase. *Nature Struct. Biol.* 4:36–39.

Carlier, M. F. 1991. Actin: protein structure and filament dynamics. *J. Biol. Chem.* 226:1–4.

Clarke, F. M., and C. J. Masters. 1975. On the association of glycolytic enzymes with structural proteins of skeletal muscle. *Biochim. Biophys. Acta*. 381:37–46.

DalleDonne, I., A. Milzani, and R. Colombo. 1997. Actin assembly by cadmium ions. *Biochim. Biophys. Acta*. 1357:5–17.

Gabdoulline, R. R., and R. C. Wade. 1997. Simulation of the diffusional association for barnase and barstar." *Biophys. J.* 72:1917–1929.

Gustafson, C. 1996. Glycolytic enzyme interactions with wild type and mutant *Saccharomyces cervisiae* actin: comparison with skeletal muscle actin. M.S. thesis. University of North Dakota, Grand Forks, ND.

Holmes, K. C., D. Popp, W. Gebhard, and W. Kabsch. 1990. Atomic model of the actin filament. *Nature*. 347:44–49.

Kabsch, W., H. G. Mannherz, D. Suck, E. F. Pai, and K. C. Holmes. 1990. Atomic structure of the actin: DNase I complex. *Nature*. 347:37–44.

Klapper, I., R. Hagstrom, R. Fine, K. Sharp, and B. Honig. 1986. Focusing of electric field in the active site of Cu-Zn superoxide dismutase: effects of ionic strength and amino-acid modification. *Proteins*. 1:47–59.

Knull, H., and J. Walsh. 1992. Association of glycolytic enzymes with cytoskeleton. *Curr. Top. Cell. Reg.* 33:15–30.

Lakatos, S., and A. P. Minton. 1991. Interactions between globular proteins and F-actin in isotonic saline solution. *J. Biol. Chem.* 266:18707–18713.

Lorenz, M., D. Popp, and K. C. Holmes. 1993. Refinement of the F-actin model against x-ray fiber diffraction data by the use of a directed mutation algorithm. *J. Mol. Biol.* 234:826–836.

Magri, E., M. Zaccarini, and E. Grazi. 1978. Versatility of G-actin as the building block of biological structures. *FEBS Lett.* 89:279–278.

Matthew, J. B. 1985. Electrostatic effects in proteins. *Annu. Rev. Biophys. Biophys. Chem.* 14:387–417.

Nakagawa, T., and F. Nagayama. 1989. Interaction of fish muscle glycolytic enzymes with F-actin and actomyosin. *Nippon Suisan Gakkaishi*. 55:165–171.

Northrup, S. H., J. Boles, and J. Reynolds. 1988. Brownian dynamics of cytochrome c and cytochrome c peroxidase association. *Science*. 241: 67–70.

Northrup, S. H., T. Laughner, G. Stevenson. 1997. MacroDox Macromolecular Simulation Program. Tennessee Technological University, Department of Chemistry, Cookeville, TN.

Northrup, S. H., J. Luton, J. Boles, and J. Reynolds. 1987. Brownian dynamics simulation of protein association. *J. Comput. Aided Mol. Des.* 1:291–311.

Northrup, S. H., K. A. Thomasson, C. M. Miller, P. D. Barker, L. D. Eltis, J. G. Guillemette, S. C. Inglis, and A. G. Mauk. 1993. Effects of charged amino acid mutations on the bimolecular kinetics of reduction of yeast iso-1-ferricytochrome c by bovine ferrocytochrome $b_5$. *Biochemistry*. 32:6613–6623.

O'Reilly, G., and F. Clarke. 1993. Identification of an actin binding region in aldolase. *FEBS Lett.* 321:69–72.

Page, R., U. Lindberg, and C. E. Schutt. 1998. Domain motions in actin. *J. Mol. Biol.* 280:463–474.

Shire, S. J., G. I. H. Hanania, and F. R. N. Gurd. 1974. Electrostatic effects in myoglobin: hydrogen ion equilibria in sperm whale ferrimyoglobin. *Biochemistry*. 13:2967–2974.

Stewart, M., D. J. Morton, and F. M. Clarke. 1980. Interaction of aldolase with actin-containing filaments: structural studies. *Biochem. J.* 1986: 99–104.

Sygusch, J., D. Beaudry, and M. Allaire. 1987. Molecular architecture of rabbit skeletal muscle aldolase at 2.7-Å resolution. *Proc. Natl. Acad. Sci. U.S.A*. 84:7846–7850.

Tanford, C., and J. G. Kirkwood. 1957. Theory of protein titration curves. I. General equations for impenetrable spheres. *J. Am. Chem. Soc.* 79: 5333–5339.

Tanford, C., and R. Roxby. 1972. Interpretation of protein titration curves: application to lysozyme. *Biochemistry*. 11:2192–2198.

Thomasson, K. A., T. Baumgartner, J. Czlapinski, T. Kaldor, and S. H. Northrup. 1997. Free energy of nonspecific binding of cro repressor protein to DNA. *J. Phys. Chem. B.* 101:9127–9136.

Tirion, M. M., D. ben-Avraham, M. Lorenz, and K. C. Holmes. 1995. Normal mode as refinement parameters for the F-actin model. *Biophys. J.* 68:5–12.

Walsh, J. L, and H. R. Knull. 1988. Heteromerous interactions among glycolytic enzymes and of glycolytic enzymes with F-actin: effects of poly(ethylene glycol). *Biochem. Biophys. Acta*. 952:83–91.

Walsh, T. P., D. J. Winzor, F. M. Clarke, and C. J. Masters. 1980. Binding of aldolase to actin-binding filaments: evidence of interaction with regulatory proteins of skeletal muscle. *Biochem. J.* 1986:89–98.

Wang, J., A. J. Morris, D. R Tolau, and L. Pagliaro. 1996. The molecular nature of the F-actin binding activity of aldolase revealed with site-directed mutants. *J. Biol. Chem.* 271:6861–6865.

Warwicker, J., and H. C. Watson. 1982. Calculation of the electric potential in the active site cleft due to $\alpha$-helix dipoles. *J. Mol. Biol.* 157:671–679.

Weiner, S. J., P. A. Kollman, D. A. Case, U. C. Singh, C. Ghio, G. Alagona, S. Profeta, Jr., and P. Weiner. 1984. A new force field for molecular mechanical simulation of nucleic acids and proteins. *J. Am. Chem. Soc.* 106:765–784.

Weiner, S. J., P. A. Kollman, D. T. Nguen, and D. A. Case. 1986. An all atom force field for simulations of proteins and nucleic acid. *J. Comp. Chem.* 7:230–252.